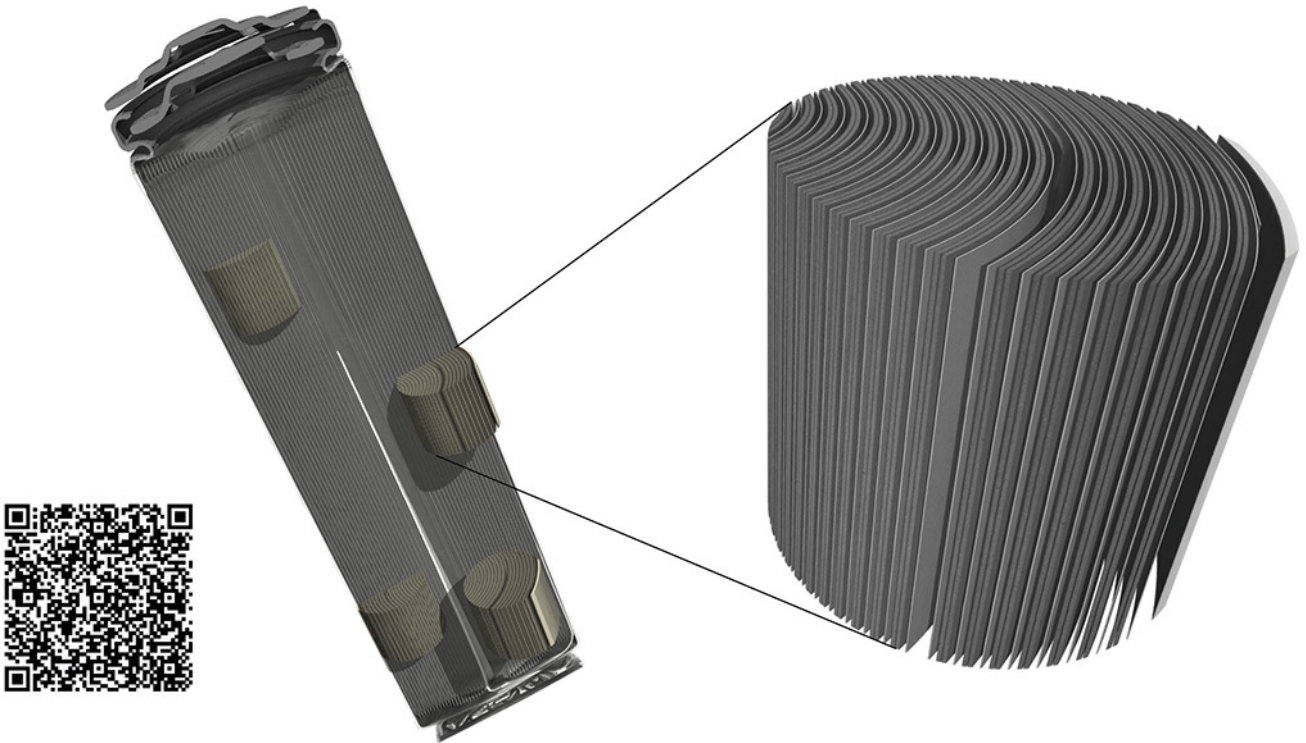


TESCAN micro-CT solutions

for energy storage materials research



TESCAN UniTOM XL

- ✓ Multi-scale non-destructive 3D imaging optimized to maximize throughput and contrast
- ✓ Fast scanning and high sample throughput with temporal resolutions below 10 seconds
- ✓ Wide array of samples types
- ✓ Enables dynamic tomography and *in-situ* experiments
- ✓ Dynamic screening for synchrotron beamtime
- ✓ Modular and open system with unmatched flexibility for research



[Click and find out more](#)

Mechanistic Insights into the Pre-Lithiation of Silicon/Graphite Negative Electrodes in “Dry State” and After Electrolyte Addition Using Passivated Lithium Metal Powder

Peer Bärmann, Marvin Mohrhardt, Joop Enno Frerichs, Malina Helling, Aleksei Kolesnikov, Sina Klabunde, Sascha Nowak, Michael Ryan Hansen, Martin Winter,* and Tobias Placke*

Because of its high specific capacity, silicon is regarded as the most promising candidate to be incrementally added to graphite-based negative electrodes in lithium-ion batteries. However, silicon suffers from significant volume changes upon (de-)lithiation leading to continuous re-formation of the solid electrolyte interphase (SEI) and ongoing active lithium losses. One prominent approach to compensate for active lithium losses is pre-lithiation. Here, the “contact pre-lithiation” of silicon/graphite (Si/Gr) negative electrodes in direct contact with passivated Li metal powder (PLMP) is studied, focusing on the pre-lithiation mechanism in “dry state” and after electrolyte addition. PLMP is pressed onto the electrode surface to precisely adjust the degree of pre-lithiation (25%, 50%, and 75%). By in situ XRD and ex situ ^7Li NMR studies, it is proven that significant lithiation of Si/Gr electrodes occurs by direct contact to Li metal, that is, without electrolyte. After electrolyte addition, de-lithiation of silicon and graphite is confirmed, resulting in SEI formation. The amount of Li metal highly impacts the presence and durability of the Li_xC and Li_xSi phases. Finally, the challenges for homogeneous pre-lithiation and SEI formation are identified, and the impact of electrolyte addition is assessed by analysis of the lateral and in-depth lithium distribution within the Si/Gr electrode.

1. Introduction

Lithium-ion batteries (LIBs) have conquered the consumer electronics as a reliable, portable power source due to their outstanding properties, including high energy and power densities, high lifetime as well as their low cost per energy content. However, further improvements in terms of energy density (Wh L^{-1}) and power density (W L^{-1}) are needed for LIBs to enable a broad market penetration of electric vehicles by competing with conventional, combustion-powered vehicles with respect to driving range and fast charging.^[1]

Silicon (Si) offers an almost ten times higher specific capacity than state-of-the-art graphite and is the most promising negative electrode material for LIBs. However, Si exhibits large volume changes upon (de-)lithiation, which hinders the broad commercialization of negative electrodes with significant amounts of Si (i.e., ≥ 10 wt%) so far. The volume


changes occurring during charge/discharge cycling result in Si particle cracking, electrode expansion and in the constant breakage and re-formation of the solid electrolyte interphase (SEI), leading to constant active lithium loss (ALL) and electrolyte consumption.^[2] A prominent concept to address the severe volume changes is the reduction of the Si particle size. Due to their size, Si nanoparticles exhibit less particle cracking, pulverization and a reduced dynamic SEI formation and, thus, are favorable for application in LIB negative electrodes. However, the large specific surface area of Si nanoparticles leads to a high ALL in the initial charge/discharge cycles.^[3] Pre-lithiation is considered as a supporting processing step for compensation of ALL and, thus, for successful application of Si nanoparticles in negative electrodes. There are various pre-lithiation methods, and each approach has certain benefits and challenges. These approaches can generally be categorized into three distinctive techniques, that is, chemical, electrochemical, and “contact” pre-lithiation, which can be typically performed before cell assembly (i.e., during negative electrode manufacturing), while few approaches also allow an in situ pre-lithiation (i.e., during cell operation).^[4]

P. Bärmann, M. Mohrhardt, M. Helling, A. Kolesnikov, Dr. S. Nowak, Prof. M. Winter, Dr. T. Placke

University of Münster
MEET Battery Research Center
Institute of Physical Chemistry
Corrensstr. 46, 48149 Münster, Germany
E-mail: tobias.placke@uni-muenster.de

J. E. Frerichs, S. Klabunde, Prof. M. R. Hansen
University of Münster
Institute of Physical Chemistry
Corrensstr. 30, 48149 Münster, Germany

Prof. M. Winter
Helmholtz Institute Münster
IEK-12
Forschungszentrum Jülich GmbH
Corrensstr. 46, 48149 Münster, Germany
E-mail: m.winter@fz-juelich.de

 The ORCID identification number(s) for the author(s) of this article can be found under <https://doi.org/10.1002/aenm.202100925>.

© 2021 The Authors. Advanced Energy Materials published by Wiley-VCH GmbH. This is an open access article under the terms of the Creative Commons Attribution License, which permits use, distribution and reproduction in any medium, provided the original work is properly cited.

DOI: 10.1002/aenm.202100925

In this work, the “contact pre-lithiation approach” by direct contact to lithium (Li) metal is investigated to unravel the pre-lithiation behavior of silicon/graphite (Si/Gr) electrodes. The main driving force for pre-lithiation is attributed to the potential difference between Li metal and the Si/Gr active materials of the negative electrode, leading to a flow of electrons in precisely this direction. To ensure charge conservation, Li^+ ions from Li metal follow the electrons into the active materials and, in turn, pre-lithiate the Si/Gr negative electrode.^[5]

While it is possible to carry out the pre-lithiation via direct contact with Li metal foil, pre-lithiation with passivated Li metal powder (PLMP) is one of the most reported methods in literature.^[6] Jarvis et al. introduced the use of PLMP to pre-lithiate the negative electrode,^[7] while PLMP benefits from its protective layer, allowing for the safe handling under dry air, in contrast to non-treated Li metal powder, which is only stable under inert conditions. The protective layer of PLMP usually consists of electronically non-conductive Li_2CO_3 .^[5a,8] Consequently, the PLMP particles must be activated before cell assembly by applying pressure, which cracks the Li_2CO_3 shell and enables the contact between the Li metal core and the electrode active material. There are different ways to perform pre-lithiation with PLMP. One route is to prepare a PLMP-based paste, which is coated on the surface of the electrode, either by a blade or with help of an airbrush.^[9] While there is no need to make changes for the conventional electrode manufacturing process, extra processing solvent and stabilizers are required to maintain a uniform distribution for longer period. Another approach is the addition of PLMP into the electrode paste, a process, which displays its own advantages and disadvantages.^[7] On the one hand, no additional processing step is needed, but on the other hand, PLMP is not stable in contact with common processing solvents and binders used in electrode preparation, such as water and polyacrylic acid (PAA) binders. Therefore, other solvents (e.g., toluene or heptane) and binders (e.g., styrene butadiene rubber) are needed.^[10] Another method is the dry addition of PLMP onto the electrode surface. While no extra solvent is needed, static forces result in challenges for achieving a homogenous distribution. In this work, PLMP is added in the dry state onto the electrode to eliminate any additional influencing parameters and, therefore, to simplify the investigation.^[11]

Regarding the lithiation reactions and kinetics, Xu et al. observed the lithiation of tin and Si/Gr negative electrodes by contact to Li metal foil alone, while no electrolyte was added.^[12] Their research mostly focused on the lithiation of tin and the impact of pre-lithiation on the electrochemical performance and stability and rather on the underlying mechanism in dry state. Forney et al. used PLMP for the pre-lithiation of Si-carbon nanotube-based negative electrodes and found potential differences occurring even after 20 h, while impedance measurements showed an ongoing reaction even after 40–50 h.^[13]

There are several factors having an impact on the pre-lithiation behavior when Li metal is used, for example it is already shown that the amount of Li metal significantly influences the pre-lithiation behavior.^[11] In addition, it is very likely that the choice of active material and particle size can influence the underlying lithiation mechanism and the cycling behavior.^[7,14]

This work focuses on unraveling the pre-lithiation mechanism for Si/Gr negative electrodes during contact pre-lithiation,

that is, by direct contact to PLMP. The impact of the carbonate-based liquid electrolyte on the reaction mechanism is explored, so that the pre-lithiation behavior in the “dry state” and after electrolyte addition can be evaluated and compared. Additionally, the amount of PLMP is varied from 25% (“PreLi25”) to 50% (“PreLi50”) and 75% (“PreLi75”), based on the theoretical capacity of the Si/Gr electrode. First, the pre-lithiation behavior is investigated by observing the electrochemical behavior in the formation cycles. Second, bulk analysis of the Si/Gr electrode is conducted to study the pre-lithiation behavior in the “dry state” as well as in the “wet state” (addition of electrolyte). Finally, the peripheral and lateral lithium distribution within the negative electrode is evaluated to clarify the homogeneity of pre-lithiation.

2. Results and Discussion

2.1. Optical and Morphological Changes of PLMP at the Surface of Si/Gr Electrodes

The pre-lithiation process of Si/Gr negative electrodes can be well observed over time by optical changes at the electrode surfaces, as representatively shown for the PreLi50 electrodes (Figure 1a–c). Shellikeri et al. studied the pre-lithiation of carbon anodes, comparing stabilized lithium metal powder and Li metal stripes as lithium sources.^[6] They also observed the optical changes during pre-lithiation, however, they directly added electrolyte to the electrodes. In our study, we analyzed the morphological changes after pressure activation (Figure 1a), after 24 h rest in the dry state (Figure 1b) and after electrolyte addition and another 48 h rest period (Figure 1c). It can be clearly observed that the shiny Li metal deposits already disappear to a large extent even without addition of electrolyte. After electrolyte addition and 48 h rest, the Li metal deposits cannot be clearly observed anymore, while the residues of the PLMP particles can be seen, that is, the Li_2CO_3 coating residues (Figure 1c).

The surface and cross-section morphology of the Si/Gr electrodes is also characterized by scanning electron microscopy (SEM), as presented in Figure 1d–g and Figure S1, Supporting Information. It can be recognized that Li metal is not completely homogeneously distributed at the electrode surface (Figure 1d). While there are areas of high Li metal (PLMP) content, covering the complete electrode surface, there are still areas of the negative electrode which are not covered. In the dry state, the pressed PLMP particles and the corresponding Li metal are still observable, as shown in Figure 1d,f. Li metal vanishes after electrolyte contact (Figure 1e,g), leaving the Li_2CO_3 coating at the surface.

A closer look at the PLMP particles reveals the coverage of the active composite material with a thin coating at the boundary. The Si particles peripheral from the PLMP particle exhibit “hard edges”, as shown in Figure 1 II (enhanced image from Figure 1d). Si particles near the PLMP particles have grown in size and the “hard edges” became spherical (Figure S1 I, Supporting Information, enhanced image from Figure 1d). These morphological changes indicate lithiation and, thus, the phase transformation of crystalline silicon (c-Si)

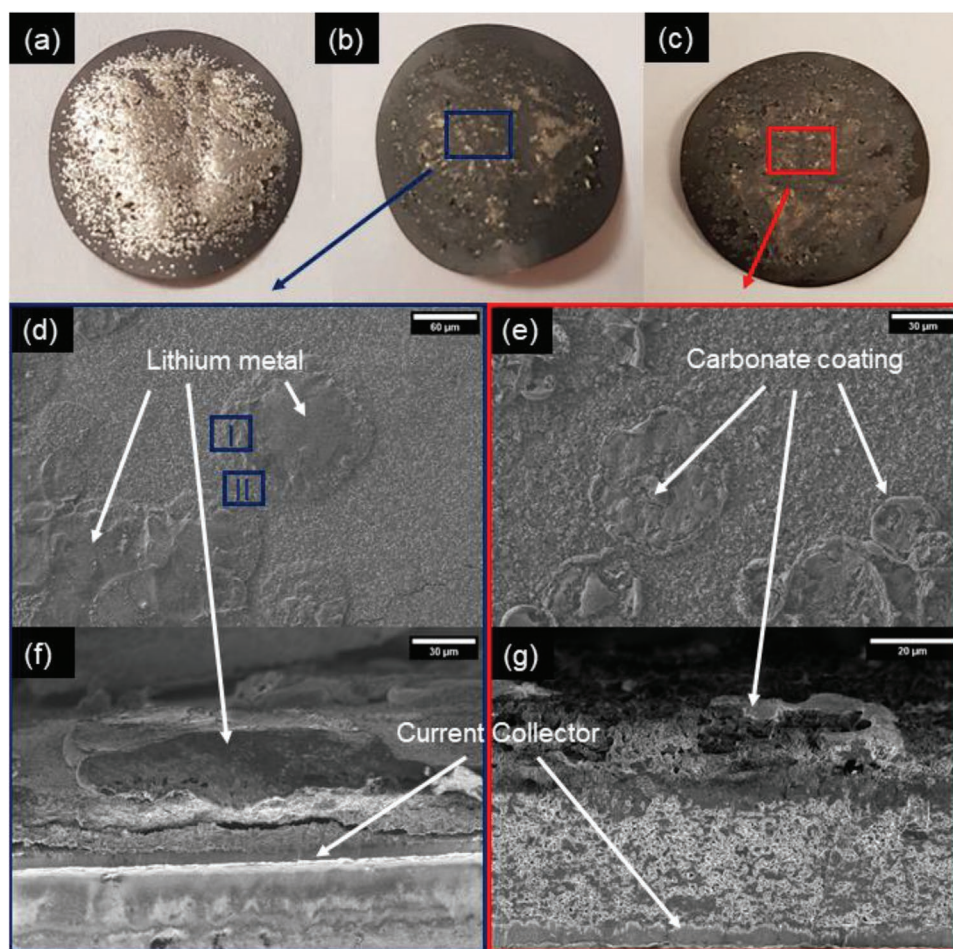


Figure 1. Photographs and SEM images of the PreLi50 Si/Gr electrodes. Photographs of the electrodes a) directly after pressure-activation, b) after 24 h rest in the dry state, and c) after the addition of electrolyte for 48 h. d–g) SEM images of pressure-activated Si/Gr electrodes (PreLi50): d) electrode surface (dry state), here the areas of Figure S1, Supporting Information, are marked with roman numbers I and II, e) electrode surface after electrolyte addition, f) electrode cross-section after pressure activation (dry state), g) electrode cross-section after electrolyte addition.

to amorphous lithiated silicon ($a\text{-Li}_x\text{Si}$) or even $c\text{-Li}_{15}\text{Si}_4$. On the other hand, the graphite flakes show no significant changes in morphology compared to the pristine electrode. From the cross-section image, shown in Figure 1d, it can be seen that partial cracking of the Si/Gr electrode occurred, which can be due to the pressure-activation step or due to lithiation, as the huge volume changes of Si may lead to pulverization of the negative electrode.

2.2. Electrochemical Behavior of Pre-Lithiated Si/Gr Electrodes

Following the 24 h rest period in dry state (without electrolyte) after pressure-induced activation of PLMP at the electrode surfaces, the Si/Gr electrodes were electrochemically investigated. The addition of electrolyte to the pre-lithiated Si/Gr electrodes within the three-electrode cell should further increase the degree of pre-lithiation of the active materials via Li^+ transport through the electrolyte. Simultaneously, due to the thermodynamic instability of the electrolyte components at the low potentials (versus $\text{Li}|\text{Li}^+$) of the Si/Gr electrode, consisting of the (pre-)

lithiated active materials as well as Li metal residues at the top of the electrode, electrolyte decomposition and SEI formation should take place. Therefore, two competing reactions should occur simultaneously, that is, i) pre-lithiation of the active materials and ii) de-lithiation of the Si and Gr active materials by SEI formation, which also results in consumption of active lithium.

Open-circuit potential (E_{OCP}) curves were recorded for the first 200 h after cell assembly (and electrolyte addition) to deduct the electrochemical stability of the Si/Gr electrodes pre-lithiated in dry state (Figure 2a). Further, cyclic voltammetry was conducted to decipher the lithiated species present, after additional 48 h in contact with electrolyte (Figure 2b). Additionally, galvanostatic cycling was performed, which is discussed in detail in Figure S2, Supporting Information.

First, higher amounts of PLMP lead to an overall lower working electrode (WE) potential after cell assembly ($t = 0$ h), as shown in Figure 2a. The lower measured WE potential can be due to a higher degree of lithiation of the active materials and/or due to an increased contribution of the residual Li metal at the electrode surface. Nevertheless, the potential rises over time for all Si/Gr electrodes, indicating an ongoing formation

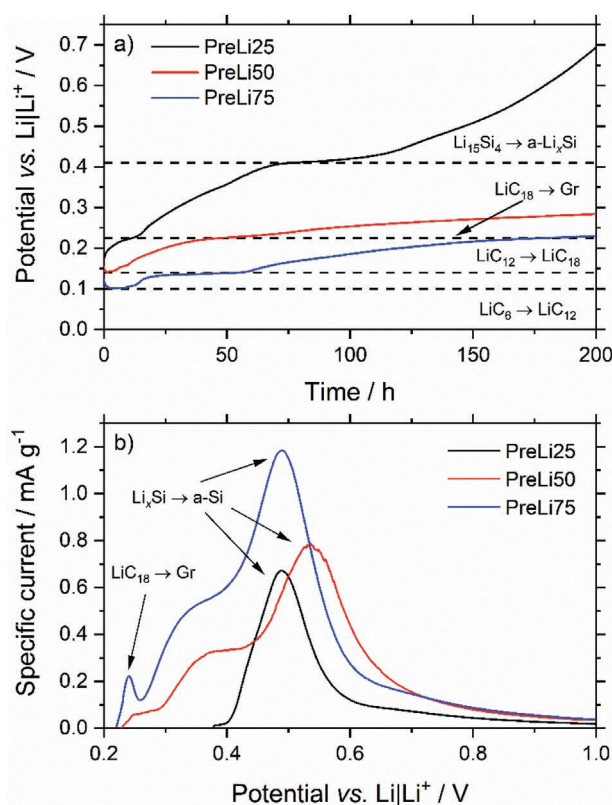


Figure 2. Electrochemical analyses of pre-lithiated Si/Gr electrodes in dependence of the degree of pre-lithiation. a) Open circuit potential (E_{OCP}) versus $\text{Li}|\text{Li}^+$ of the WE recorded in Si/Gr || Li metal cells (half-cell setup, three-electrode configuration) after pre-lithiation with different amounts of PLMP (25%, 50%, and 75%) and a rest period of 24 h in dry state (without electrolyte). b) De-lithiation behavior of Si/Gr electrodes after 24 h rest step in dry state and additional 48 h rest with electrolyte during the first discharge in cyclic voltammetry measurements. The de-lithiation potentials versus $\text{Li}|\text{Li}^+$ of the corresponding phases are well in agreement with literature.^[16]

of lower lithiated silicon/graphite phases, due to electrolyte decomposition and most likely due to self-discharge of the active materials, resulting in SEI formation.^[15]

In addition, the Si/Gr electrodes for all investigated degrees of pre-lithiation exhibit plateaus at potentials, which are marked in Figure 2a.^[16] For the highest pre-lithiated electrode (PreLi75), the first plateau appears at ≈ 140 mV versus $\text{Li}|\text{Li}^+$, which corresponds to the de-lithiation potential of the phase transformation from LiC_{12} to LiC_{18} and approaches a limit of ≈ 230 mV versus $\text{Li}|\text{Li}^+$ after 200 h. A potential plateau at ≈ 220 mV versus $\text{Li}|\text{Li}^+$ is also observable for the other two pre-lithiated electrodes. For PreLi50, however, the plateau is present for almost 24 h, while for PreLi25 the duration decreases to only ≈ 5 h. The former one reaches a boundary value of ≈ 280 mV versus $\text{Li}|\text{Li}^+$, while the lowest pre-lithiated electrode still shows a strong potential increase even after 200 h with electrolyte contact. The de-lithiation potential plateau at 220 mV versus $\text{Li}|\text{Li}^+$ corresponds to the transformation from the LiC_{18} phase to lower-lithiated Li_xC_6 ($x < 0.33$) phase (Figure 2a), indicating the presence of this phase for all investigated degrees of pre-lithiation. However, the highest lithiated

electrode reaches this phase in equilibrium after 200 h, while the phase vanishes in the first 24 h for the PreLi25 electrode. Furthermore, PreLi25 shows a large plateau at ≈ 420 mV versus $\text{Li}|\text{Li}^+$ for more than 40 h, which is characteristic for the de-lithiation of the crystalline (c-) $\text{Li}_{15}\text{Si}_4$ phase to a lower lithiated amorphous (a-) Li_xSi phase. Afterward, a steep increase in potential is observed, which can be assigned to the de-lithiation of the lower lithiated a- Li_xSi phase(s).^[15]

The differently pre-lithiated Si/Gr electrodes are de-lithiated from their individual E_{OCP} by cyclic voltammetry after electrolyte contact for 48 h (Figure 2b). When the pre-lithiated Si/Gr composites are de-lithiated, the characteristic peak at a potential of ≈ 0.45 V versus $\text{Li}|\text{Li}^+$, which corresponds to the transformation of the c- $\text{Li}_{15}\text{Si}_4$ phase to the a- Li_xSi phase, is observable for all pre lithiated electrodes.^[16a] However, for the PreLi50 electrode, the characteristic current peak is shifted to 0.5 V versus $\text{Li}|\text{Li}^+$, which might be influenced by residual Li metal. As already described above, the potential of PreLi75 after 200 h is below the potential for the phase transformation of LiC_{18} to Li_xC_6 ($x < 0.33$) after 48 h, thus, the de-lithiation peak at ≈ 220 mV versus $\text{Li}|\text{Li}^+$ is still observable in Figure 2b. For lower pre-lithiated Si/Gr electrodes, this peak is not present, which is consistent with the conclusions drawn by analyzing the E_{OCP} curves (Figure 2a).

The potential increase occurring after addition of electrolyte (Figure 2a) can be explained by the decomposition of electrolyte to form a SEI layer: On the one hand, Li metal is consumed for SEI formation and, on the other hand, lithiated silicon and graphite phases will be de-lithiated for SEI formation according to a self-discharge mechanism.^[15] Furthermore, it is very likely that the Li^+ ions move from a highly lithiated electrode surface deeper inside the electrode (toward the current collector), leading to a more homogeneous distribution of Li^+ ions and, therefore, result in an increased potential of the overall electrode, which will be further discussed below. Overall, the total Si/Gr electrode potential consists of Li metal at the electrode surface as well as lithiated and non-lithiated silicon and graphite phases, thereby, resulting in local differences of the Si/Gr electrode potential.

2.3. Analysis of Bulk Properties of Pre-Lithiated Si/Gr Electrodes by In Situ XRD and Ex Situ Solid-State ^7Li NMR

Bulk analysis of the Si/Gr electrodes was conducted by in situ X-ray diffraction (XRD) (Figures 3 and 4) and ex situ solid-state ^7Li nuclear magnetic resonance (NMR) studies (Figures 5 and 6). For XRD analyses, PLMP was pressed on top of the electrode and directly transferred into the in situ cell with the Si/Gr active materials facing the Be disk and measured for 24 h in dry state after assembly (Figure 3). Afterward, the electrolyte was filled into the cell and the measurement was resumed for 48 h (Figure 4). This procedure was repeated for all Si/Gr electrodes in the same way and analyzed with regard to the different degrees of pre-lithiation.

As displayed in Figure 3, the characteristic reflections of graphite (002) at $2\theta \approx 26.8^\circ$ and of the ordered (111) planes of crystalline silicon (c-Si) at $2\theta \approx 28.6^\circ$ are observable at the beginning of the measurement in the dry state for all Si/Gr

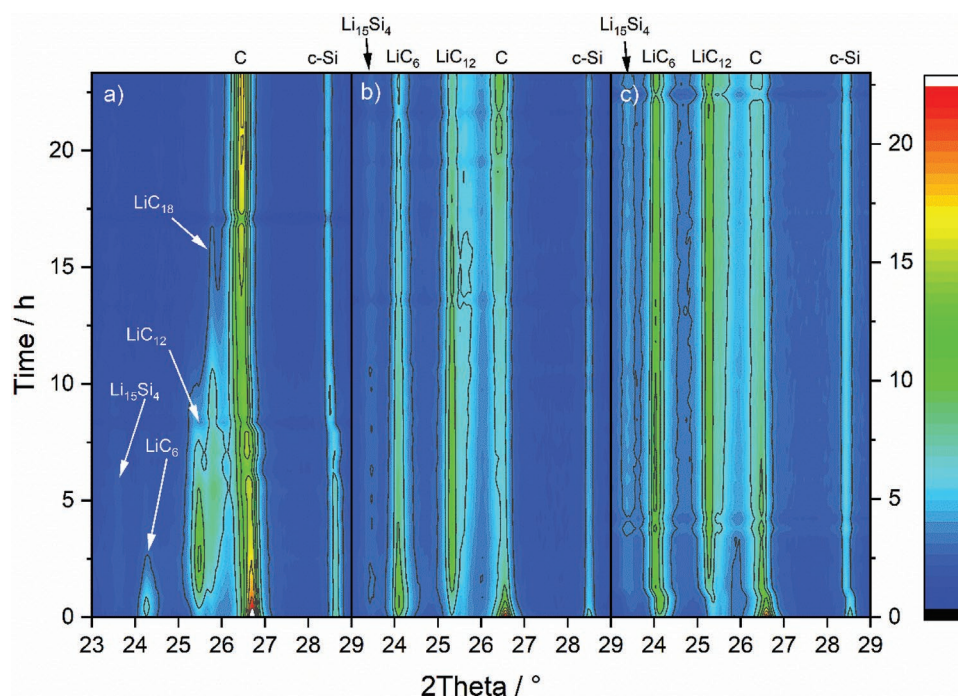


Figure 3. In situ XRD analyses of Si/Gr electrodes in dependence of the degree of pre-lithiation using PLMP (dry state, without electrolyte). Analysis of a) PreLi25, b) PreLi50, and c) PreLi75 electrodes in the dry state for 24 h. The corresponding lithiated phases are labeled accordingly, hereby, “C” relates to the (002) reflection of graphite and c-Si to the (111) reflection of crystalline silicon.

electrodes.^[17] The d-lattice spacing between the graphene layers increases during lithiation, leading to a shift of the reflection to lower 2θ values. In the first hour of the measurement, all reflections for the lithiated graphite can be observed in all investigated electrodes, namely $2\theta \approx 24.1^\circ$ for the highest lithiated LiC_6

phase, $2\theta \approx 25.3^\circ$ for LiC_{12} and $2\theta \approx 25.8^\circ$ for LiC_{18} .^[17a] The latter phase overlaps with a small residual peak, originating from the in situ cell parts, as observed in reference measurements (Figure S3, Supporting Information). While the intensity of the fully lithiated graphite phase increases with time, the intensity

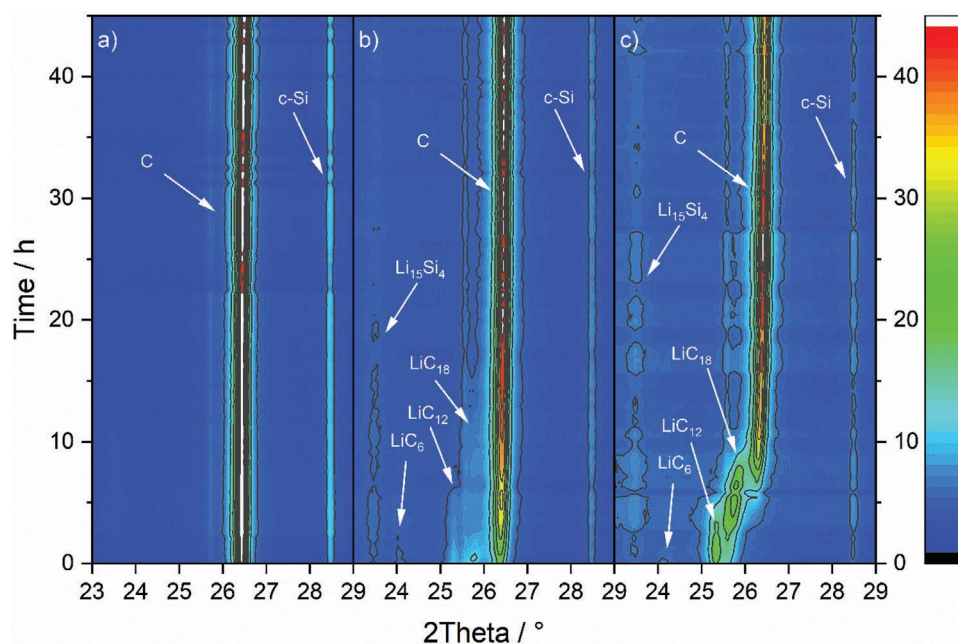


Figure 4. In situ XRD analyses of Si/Gr electrodes in dependence of the degree of pre-lithiation using PLMP (after addition of electrolyte). Analysis of a) PreLi25, b) PreLi50, and c) PreLi75 electrodes after the addition of the electrolyte, recorded for 48 h. The corresponding lithiated phases are labeled accordingly, hereby, “C” relates to the (002) reflection of graphite and c-Si to the (111) reflection of crystalline silicon.

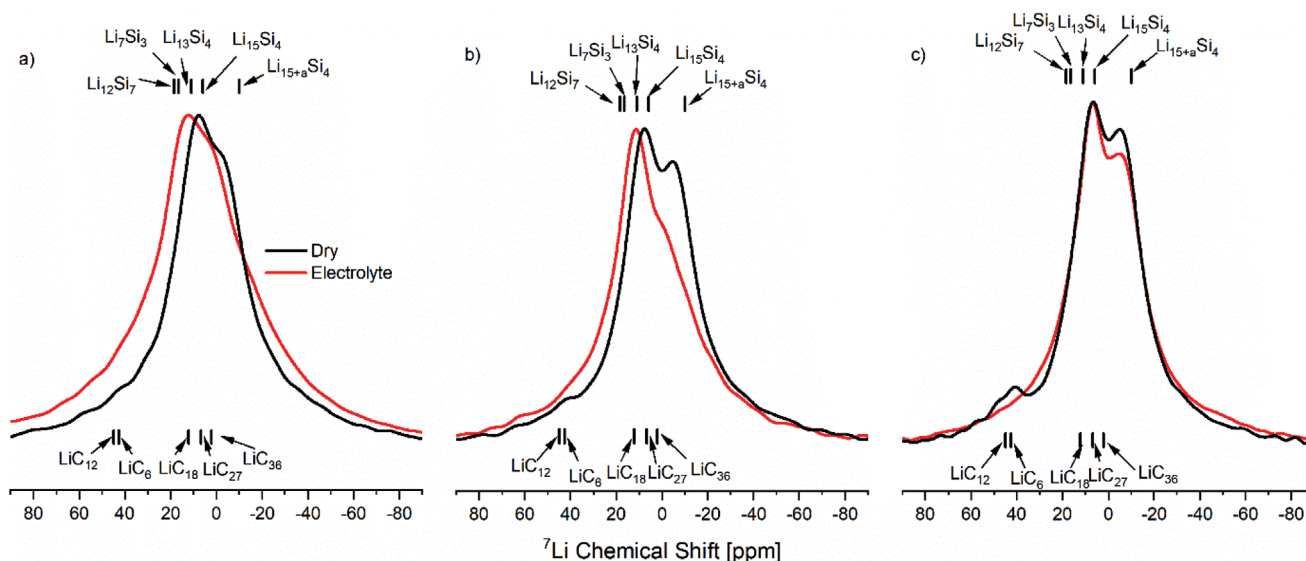


Figure 5. Ex situ solid-state ^7Li NMR analyses of Si/Gr electrodes in dependence of the degree of pre-lithiation using PLMP. Analysis of a) PreLi25, b) PreLi50, and c) PreLi75 electrodes in their dry state (after 24 h; black curve) and after electrolyte addition (additional 48 h; red curve). The lithiated phases are labeled accordingly and an overview of the corresponding chemical shifts can be found in Table S1, Supporting Information.

of the pristine graphite reflection decreases. The same phenomenon can be noticed for silicon in all samples. While the intensity of c-Si decreases, a reflection at $2\theta \approx 23.5^\circ$ appears, which is characteristic for c- $\text{Li}_{15}\text{Si}_4$, the highest lithiated silicon phase. The other distinctive reflections of this phase can also

be seen at $2\theta \approx 20.5^\circ$ and $2\theta \approx 39.8^\circ$ (see also Figure S3, Supporting Information).^[18]

All lithiated phases discussed above can be observed throughout the whole XRD measurement period (24 h) for the PreLi50 and PreLi75 electrodes (Figure 3b,c). In contrast,

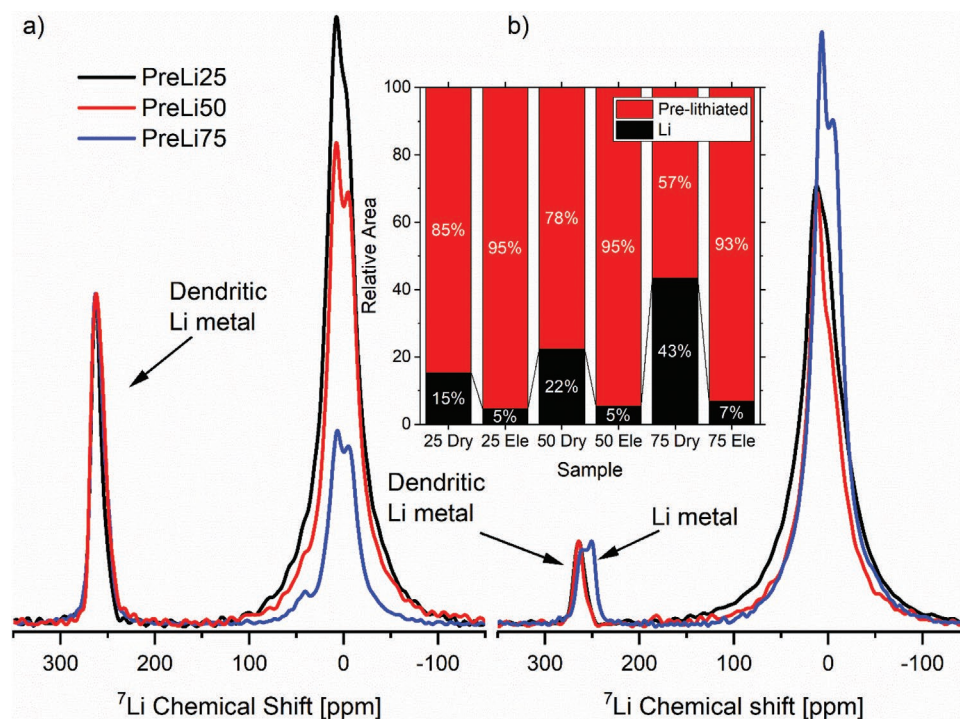


Figure 6. Static ^7Li NMR spectra of pre-lithiated Si/Gr electrodes in dependence of the degree of pre-lithiation using PLMP. a) Dry state after 24 h and b) after electrolyte addition and additional 48 h. The inset shows the relative areas (integrals) of the Li metal and the pre-lithiated Si/Gr electrodes (dry state and after addition of electrolyte). All spectra are normalized to the ^7Li metal signal.

the PreLi25 electrode exhibits a distinctively different behavior (Figure 3a). First, the lithiation can be clearly seen within the first hour by appearance of the highest lithiated phases, namely LiC_6 and $\text{c-Li}_{15}\text{Si}_4$. In contrast to the PreLi50 and PreLi75 electrodes, de-lithiation is detected as the lithiated graphite phases LiC_6 , LiC_{12} and LiC_{18} vanish after 2.5, 10, and 17.5 h, respectively (Figure 3a). Additionally, $\text{c-Li}_{15}\text{Si}_4$ cannot be differentiated from the “background noise” after 7.5 h, also indicating a de-lithiation process. As no electrolyte is present in these “dry state” measurements, the disappearance of the highly lithiated phases can only be explained either by the lithiation of neighboring and electronically-connected, non-lithiated silicon, and graphite particles through the highly lithiated particles.^[15,19] It also has to be kept in mind that any amorphous $\text{a-Li}_x\text{Si}$ phases cannot be observed by XRD analysis. Another hypothesis is the inhomogeneous lithiation of the silicon and graphite particles themselves (especially close to Li metal at the top of the electrode) in the first hour of pre-lithiation, while a more homogenous degree of lithiation is reached afterward.^[14a] Tardif et al.^[19b] showed the radial lithiation of silicon nanoparticles, resulting in a partially lithiated $\text{a-Li}_x\text{Si}$ shell and a non-lithiated c-Si core, which in turn could explain the observed behavior. Moreover, the lithiation probably occurs most likely near the PLMP particles at the top of the electrode, leading to non-lithiated c-Si and graphite particles close to the current collector.

After the addition of the electrolyte to the in situ cell, a change of the present phases can be detected for all degrees of pre-lithiation, as shown in Figure 4. The presence and stability of the lithiated phases is highly dependent on the amount of Li metal used for the pre-lithiation of the Si/Gr electrodes. The insertion of electrolyte has no significant effect on the reflections detected for the PreLi25 electrode (Figure 4a). Therefore, the pre-lithiation process is most likely already completed without the addition of any electrolyte with regard to the presence of lithiated phases.

For the higher pre-lithiated electrodes, de-lithiation of silicon and graphite can be clearly seen, as discussed above for the electrochemical characterization (Figure 2a). The reflection at $2\theta \approx 24.1^\circ$ (LiC_6) quickly vanishes for both degrees of pre-lithiation (Figure 4b,c), likewise, the reflection at $2\theta \approx 25.3^\circ$ (LiC_{12}) mostly disappeared after 5 h. As predicted by the investigation of the E_{OCP} curves of the pre-lithiated electrodes, the lowest lithiated graphite phase (LiC_{18}) is still observable for both samples after 48 h at $2\theta \approx 25.8^\circ$, and the same holds true for the $\text{c-Li}_{15}\text{Si}_4$ phase. This pre-lithiation behavior gives evidence for the de-lithiation of graphite after the addition of the electrolyte to form the SEI, while the highly lithiated silicon phase is mostly stable toward the electrolyte. This behavior is in accordance with the self-discharge mechanism of the $\text{c-Li}_{15}\text{Si}_4$ phase, since the lithiated graphite phases hinder an increase of the electrochemical potential to values at which a de-lithiation of the $\text{c-Li}_{15}\text{Si}_4$ phase would be possible, that is, at ≈ 0.42 V versus $\text{Li}|\text{Li}^+$.^[15] This phenomenon for Si/Gr electrodes is actually favorable, as a pre-lithiation of only silicon is desirable since silicon is primarily responsible for the low Coulombic efficiencies during the initial charge/discharge cycle(s).

To give further evidence, ex situ solid-state ^7Li NMR experiments using static NMR conditions were conducted, that is, 24 h after pre-lithiation in the dry state and 48 h after pre-lithi-

ation with the addition of electrolyte (Figure 5). In comparison to the XRD analyses, NMR investigations allow for a qualitative analysis of the underlying state of lithiation of silicon. We note that the NMR characterization performed here is only of a qualitative nature, as the number of phases for both the lithiated silicon and graphite combined with their ^7Li chemical shift range does not allow for a distinct fitting of the ^7Li NMR signals due severe spectral overlap between these phases. The ^7Li chemical shifts of the known lithiated phases for graphite and silicon are listed in Table S1, Supporting Information, and marked in Figure 5.^[17b,20] In general, the ^7Li resonances of lithiated graphite shift toward higher frequencies (or equivalently higher ppm values) with a higher degree of lithiation, whereas the opposite trend can be observed for the ^7Li shifts of the Li–Si intermetallic phases. Nevertheless, the ^7Li chemical shifts of the higher lithiated graphite phase should be distinguishable from the corresponding silicon phases. It should also be kept in mind that the LiPAA binder contributes to the observable ^7Li NMR signal (maximum at -6 ppm, see Figure S4b, Supporting Information); however, the contribution does not change the qualitative interpretations made here, as it can be assumed to be constant for each investigated sample. Therefore, only the observed maxima and shift positions are discussed. Additionally, an indication about the residual Li metal can be developed when taking into account the full ^7Li chemical shift range from -150 to 350 ppm (Figure 6).^[21]

As shown in Figure 5a, the PreLi25 electrode does not display the highly lithiated graphite phases (LiC_6 at 42.6 ppm and LiC_{12} at 45 ppm) after 24 h of pre-lithiation in the dry state. In contrast, the higher pre-lithiated Si/Gr electrodes, that is, PreLi50 and PreLi75, exhibit a small ^7Li signal, which reveals the presence of these phases after pre-lithiation for 24 h in the dry state (Figure 5b,c). Both of these observations are in good accordance with the in situ XRD data. After addition of the electrolyte and an extra rest period of 48 h, the highly lithiated graphite phases cannot be identified anymore. Moreover, the lower lithiated graphite phases are reported in the ^7Li chemical shift range of 0 – 10 ppm. However, in this region also ^7Li signals resulting from the LiPAA binder, Li species within the SEI, and Li–Si phases can be found. Hence, no further assumptions can be made about the lower lithiated graphite phases.^[22] Furthermore, all pre-lithiated electrodes exhibit a broad ^7Li signal at ≈ 75 ppm under dry conditions (Figure 5), indicating the lithiation of silicon to the highly lithiated $\text{c-Li}_{15}\text{Si}_4$ phase, which could also be observed in the XRD measurements (Figures 3 and 4). For the higher pre-lithiated Si/Gr electrodes (PreLi50 and PreLi75), an additional signal at a ^7Li chemical shift of ≈ -6 ppm suggests the presence of the over-lithiated $\text{Li}_{15+a}\text{Si}_4$ phase (Table S1, Supporting Information), which further indicates the presence of the $\text{c-Li}_{15}\text{Si}_4$ phase.^[17b,23] After the addition of the electrolyte, this ^7Li signal disappears for PreLi50 indicating the de-lithiation of the over-lithiated $\text{Li}_{15+a}\text{Si}_4$ phase (Figure 5b). Only a small shoulder remains at ≈ -0.8 ppm, which is expected as the SEI should be formed after the contact with the electrolyte. For the PreLi25 and PreLi50 electrodes, the ^7Li signal at ≈ 75 ppm shifts to higher values (≈ 11.5 ppm). This observation suggests the formation of a less shielded Li^+ environment. As has been shown from the in situ XRD experiments, only the LiC_{18} phase remains to some extent when considering the lithiated graphite

phases. Therefore, we assume that the main contribution of the ^7Li signal at 11.5 ppm originates from lithiated silicon phases. It can further be assumed that after the addition of electrolyte, isolated silicon ions in $\text{Li}_{15}\text{Si}_4$ start to form Si_2 dumbbells, resulting in the formation of the $\text{Li}_{13}\text{Si}_4$ phase, containing both types of structural motifs.^[17b,23] Nevertheless, the highest pre-lithiated electrode (PreLi75; Figure 5c) exhibits almost no change upon addition of the electrolyte. This shows that no significant de-lithiation of the highly lithiated silicon phase to form the SEI occurs, thus, confirming the conclusions drawn from in situ XRD analyses.

^7Li NMR also allows to study and quantify the residual Li metal content as summarized in Figure 6. Here, the relative areas/integrals are calculated to show the correlation between residual Li metal and lithiated active material (Si and Gr). All pre-lithiated Si/Gr electrodes (dry state) show ^7Li signals for Li metal at ≈ 270 ppm (Figure 6a). This ^7Li chemical shift is slightly higher compared to 250 ppm for pristine PLMP (see Figure S4a, Supporting Information), used for the pre-lithiation of the Si/Gr electrodes. Bhattacharyya et al.^[24] observed the same ^7Li chemical shift upon multiple cycles of a Li metal battery, which they assigned to dendritic Li metal. Therefore, we tentatively conclude that the pressed PLMP at the electrode surface has a morphology comparable to that of dendritic Li metal, as indicated by the ^7Li NMR measurements. We note that the signal splitting of the ^7Li signal in two signals at ≈ 250 and ≈ 260 ppm for PreLi75 (blue spectrum) may arise from the presence of different Li orientations toward the static magnetic field, which may be attributed to a separation of Li metal from the Si/Gr electrode after the scratching process used for NMR sample preparation, due to the high amount of Li present in this sample.^[25]

The relative ^7Li signal areas of the (dendritic) Li metal peaks at ≈ 270 ppm are $\approx 15\%$ for PreLi25, $\approx 22\%$ for PreLi50 and $\approx 43\%$ for PreLi75, as shown in the inset of Figure 6. These numbers suggest that higher Li metal contents at the surface lead to higher Li metal residues after the resting period of 24 h in the dry state. However, the intensity of the Li metal signal decreases significantly after contact with electrolyte (Figure 6b). Here, the Li metal peaks exhibit relative areas of only $\approx 5\%$ for the PreLi25 and PreLi50 electrodes. Since residual Li metal is identified even for the lowest pre-lithiated electrode (PreLi25) after electrolyte contact for 48 h, it seems likely that Li metal might be passivated at the surface. This effect could be caused by an effectively protecting SEI layer, resulting in slow Li^+ diffusion kinetics. In addition, the Si/Gr particles at the electrode surface could be highly lithiated, so that further in-depth lithiation into the electrode will be inhibited. Additionally, the PreLi75 electrode exhibits two ^7Li signals in the range of 270–250 ppm after addition of electrolyte, indicating that besides dendritic Li metal also pristine PLMP is apparent (Figure 6b) as discussed above.

Summarizing the bulk analyses of the pre-lithiated Si/Gr electrodes via XRD and ^7Li NMR techniques, the lithiation of graphite and silicon by simple contact to Li metal, that is, without addition of electrolyte, could be proven. In each Si/Gr electrode the highest lithiated states of both silicon ($\text{c-Li}_{15}\text{Si}_4$) and graphite (LiC_6) are reached. However, the durability of the phases highly depends on the Li metal content (degree of pre-lithiation), even though the amount of Li metal has no

significant impact on the initial reaction kinetics. After addition of the electrolyte, graphite and silicon start to de-lithiate due to electrolyte decomposition and SEI formation. Unreacted Li metal at the electrode surface then starts to form an SEI immediately after contact with the electrolyte, directing to a passivation as well as deceleration of the lithium intercalation/insertion into the active materials with increasing electrode depth (toward the current collector).

2.4. Lateral and Peripheral Pre-Lithiation Mechanism in Si/Gr Negative Electrodes

Motivated by the detection of residual Li metal through ^7Li NMR and by optical and SEM images, the pre-lithiation homogeneity was studied in lateral resolution by Raman spectroscopy. The Raman spectra were collected by mapping of an area of $60\text{ }\mu\text{m}$ in length and $28\text{ }\mu\text{m}$ in width. Each row is averaged, and the spectra are shown in a waterfall diagram in reference to the distance of a PLMP particle. The prominent crystalline silicon band at $\approx 518\text{ cm}^{-1}$ is most notably, which is assigned to the scattering of the first order transverse optical (TO) and longitudinal optical phonon modes.^[19b] Further characteristic peaks can be observed at ≈ 300 and $\approx 950\text{ cm}^{-1}$, which can be allocated to the scattering of the longitudinal acoustic mode and the second-order optical phonon mode (2TO), respectively.^[26] The G-band and D-band of graphite are observable at 1585 and 1330 cm^{-1} , respectively.^[27] All designated bands are shown in Figure S5, Supporting Information.

A series of Raman spectra of the PreLi50 electrode is shown in Figure 7a (24 h after pressing) and in Figure 7b (48 h after addition of electrolyte). The other two pre-lithiation degrees are not discussed here, since the Raman mapping is performed close to a PLMP particle, therefore, no significant changes in the lithiation behavior are assumed. After pressure activation, the band associated with c-Si is seen to diminish and disappear almost completely when going closer to the PLMP particle. This observation agrees with previous Raman measurements on Si-based negative electrodes.^[28] The bands corresponding to a-Si are not considered for this study, as only the phase transformation of c-Si is needed to make qualitative remarks about the pre-lithiation degree of silicon. Beyond $10\text{ }\mu\text{m}$ of the particle, the intensity of the silicon peak starts to fluctuate, such as in the pristine electrode (see Figure S6b, Supporting Information), which can be explained by local accumulation of silicon particles at the surface. Nevertheless, the diminishing TO band close to the PLMP particle proves the lithiation of the silicon, leading to an amorphous structure without the use of electrolyte (Figure 7a). The Raman spectra at the PLMP particle are different compared to the Si/Gr electrode surface. A broad peak between 320 and 730 cm^{-1} is observed, which can be attributed to Li_2O and the Li_2CO_3 coating of PLMP.^[29] Furthermore, an increase in background noise can be noticed for higher wavenumbers. This effect might be due to the lack of focus, because the laser is focused on the electrode surface, while the surface of the particle is slightly higher (see SEM cross-sections in Figure 1d,e).

After addition of electrolyte and a rest period of 48 h, the first three spectra close to the PLMP particle also show the

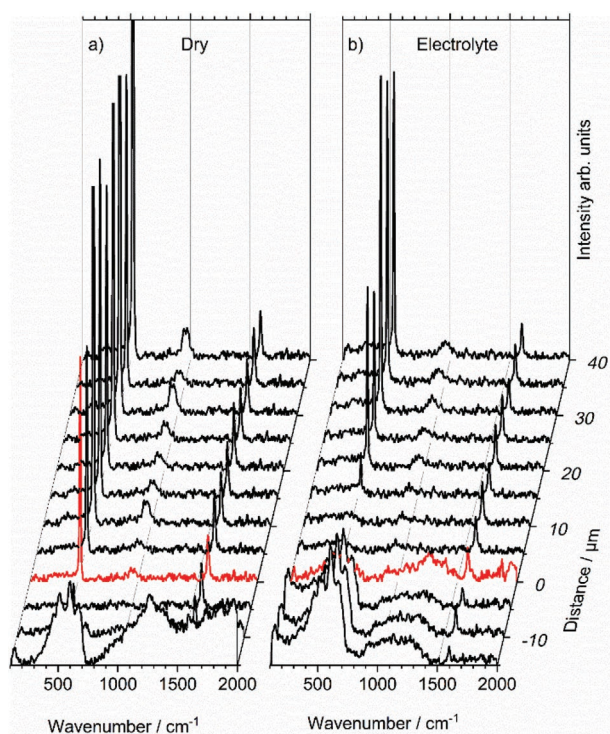


Figure 7. Raman spectra of the PreLi50 electrode close to a PLMP particle. a) After 24 h in dry state and b) after 48 h with electrolyte. The red lines display the border of the PLMP particle to the Si/Gr electrode surface. For better comparability, some intensities of the spectra in the dry state are not shown.

broad peak from 320 to 730 cm^{-1} with an individual peak at $\approx 603 \text{ cm}^{-1}$, attributed to various lithium salts (Figure 7b).^[29] The silicon band at 518 cm^{-1} is not observable until at least 15 μm away from the PLMP particle. Beyond this point, the intensity of the band increases until reaching a distance of 25 μm to the PLMP particle. During lithiation of graphite, the D-band usually disappears in the Raman spectra and a G-band doublet appears.^[27a] However, due to the high crystallinity of graphite the D-Band is not clearly visible (Figure 7), therefore, it is hard to monitor its disappearance.^[27b] The constant intensity and shape of the G-band indicates no significant change in lithiation state of graphite at least at the time of measurements at 0 h in the dry state (shown in Figure S6a, Supporting Information), after 24 h in the dry state and after additional 48 h with electrolyte (Figure 7a,b).

The laser ablation–inductively coupled plasma–optical emission spectroscopy (LA-ICP-OES) technique provides both a good lateral and in-depth resolution of the lithium distribution compared to Raman spectroscopy, which mostly focuses on lateral resolution. Moreover, it is possible to investigate whole electrodes with a diameter of several millimeters, limited only by the size of the ablation chamber.^[30] Monitoring the Cu current collector signal gives evidence about the ablation depth, and once the signal significantly increases, the ablation can be considered as complete (see Figure S7, Supporting Information). The Cu intensity rises faster for the PreLi25 electrode than for the other degrees of pre-lithiation, probably due to the higher amounts of Li metal present at the surface of the electrode.

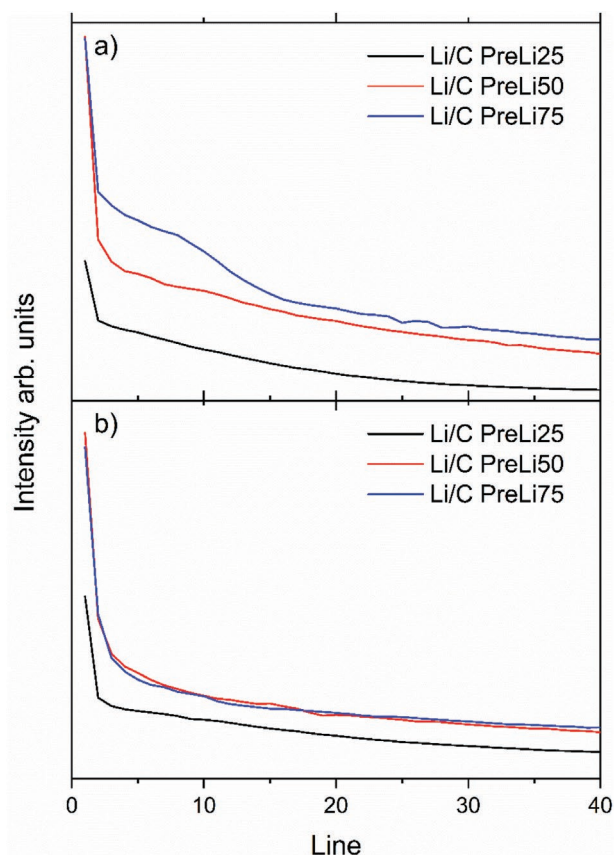


Figure 8. Averaged Li/C intensities of the first 40 lines of pre-lithiated Si/Gr electrodes from LA-ICP-OES analysis. a) Dry state for 24 h and b) after electrolyte contact for 48 h. Each ablation line had a length of 12–13 mm at the surface and is repeatedly ablated until the current collector is reached.

This phenomenon can also be locally observed at areas, where no PLMP is present regardless of the degree of pre-lithiation, as shown in Figure S8, Supporting Information. Here, areas without PLMP particles at the surface exhibit deeper and broader ablation craters through the electrode compared with areas where PLMP particles are present. This behavior is most likely due to the extra thickness when PLMP particles are pressed at the surface. Additionally, the heat of the laser could melt Li metal, leading to a flow of Li metal inside the ablation crater, which needs to be considered in the following discussion. However, monitoring the carbon signal of the electrodes still shows a constant ablation of carbon during the process, hence, the internal standard does not change during the measurement (see Figure S7, Supporting Information).

For LA-ICP-OES analysis, the same pre-lithiation times are considered as before (24 h in dry state and 48 h after electrolyte addition) and the intensity of the emission line of lithium is divided by the intensity of the carbon emission line as internal standard. As seen in Figure 8, the highest amount of Li can be detected during the first ablation and drops significantly in the following lines for all electrodes. In the dry state (Figure 8a), the highest lithiated electrode (PreLi75) exhibits higher amounts of Li after 15 lines than PreLi50, indicating a higher degree of lithiation in depth of the electrode for higher

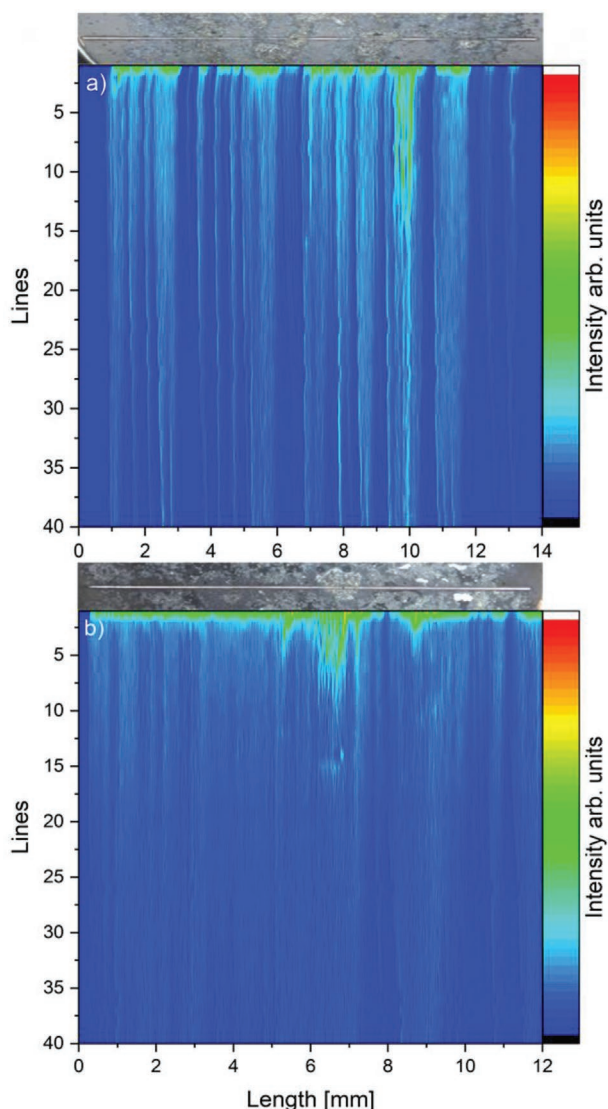


Figure 9. Li/C depth profiles of pre-lithiated Si/Gr electrodes (PreLi50) from LA ICP-OES analysis. a) In dry state after 24 h and b) after electrolyte contact for 48 h with the corresponding images of the Si/Gr electrode surfaces after the ablation process, where the line of ablation is clearly visible. All pre-lithiated samples are shown in Figure S9, Supporting Information.

Li metal amounts at the surface. Afterward, the Li metal content decreases at the same rate for all degrees of pre-lithiation. As expected, the overall amount of Li metal follows with the degree of pre-lithiation, however, there is a higher difference between PreLi50 and PreLi25 electrodes than between PreLi50 and PreLi75, which is most likely due to the higher amount of Li metal at the surface as described above. While the pre-lithiation degree can easily be controlled using PLMP as pre-lithiation agent, one major drawback is the non-homogeneous distribution, as shown in Figure 9a (PreLi50 sample, dry state) and Figure S9a,c,e, Supporting Information, (all samples in dry state). On the one hand, at points of highly accumulated PLMP particles, the amount of lithium also significantly increases in depth of the electrode. On the other hand, at areas with no

or less PLMP particles at the surface, also no or only minor amounts of lithium are detected even after several ablations, which agrees with the Raman analysis (Figure 7). When the Si/Gr electrodes are pre-lithiated to only compensate the initial ALL, the surface is probably not completely covered with Li metal, which can lead to an inhomogeneous pre-lithiation and inhomogeneous SEI formation.

The pre-lithiated electrodes after electrolyte contact for 48 h (Figure 8b) present a similar rapid drop in Li/C intensity in the first lines as observed for the dry electrodes. Additionally, the decline rate of the amount of Li is nearly the same for all electrodes, indicating an increased homogeneity of the lithium distribution within the electrode through the addition of electrolyte. Similarly, the lithium intensity in the electrodes after electrolyte contact is higher beneath the Li metal particles, also toward increased electrode depth, as observable in Figure 9b and Figure S9b,d,f, Supporting Information, (all samples after electrolyte addition). However, the lithium content is also more evenly distributed horizontally, showing a lithiation of the electrode peripheral to the PLMP particles after electrolyte contact, concurrent with the Raman analyses.

Summarizing the results of the lithium distribution analysis, the lithiation of the Si/Gr electrode preferentially occurs near the PLMP particles in the dry state, but a further peripheral lithiation can be detected after the electrolyte is added. Furthermore, a non-negligible amount of lithium is detected inside the bulk electrode, confirming the lithiation within increased electrode depth already occurs in the dry state.

3. Conclusion

The pre-lithiation mechanism of silicon/graphite (Si/Gr) composite electrodes by PLMP was successfully investigated in dependence of the degree of pre-lithiation. Various amounts of PLMP were pressure-activated at the surface of the Si/Gr electrode (25%, 50%, and 75% in relation to the electrode's theoretical capacity) and the electrodes were analyzed after 24 h in the “dry state” and after additional 48 h after contact to electrolyte (“wet state”).

First, the electrochemical stability and de-lithiation potential as well as the Coulombic efficiency in the formation cycles were investigated. The open circuit potential (E_{OCP}) and CV measurements showed that the electrochemical stability of the lithiated graphite and silicon phases is dependent on the amount of Li metal at the surface. A pre-lithiation degree of 25% of the theoretical capacity is sufficient to compensate the initial ALL in these Si/Gr model electrodes. Furthermore, the lithiation of silicon before cell assembly (dry state) leads to an activation of the electrode beforehand, that is, the associated volume changes lead to a higher porosity of the electrode and, therefore, improved wetting and higher contribution of the active materials to the reversible capacity starting from the first cycle. E_{OCP} measurements confirmed de-lithiation of silicon and graphite after electrolyte addition due to the “corrosion reaction” between electrode and electrolyte and subsequent SEI formation.

Second, bulk analysis was performed via in situ XRD and ex situ ^7Li NMR measurements. The lithiation of Si/Gr electrodes

with direct contact to Li metal was proven, thus, there is no necessity to add electrolyte for the lithiation to occur. The Li metal amount highly impacts the presence and durability of the lithiated phases of the active materials. In accordance with the E_{OCP} results, it is shown that the active materials de-lithiate to form the SEI after electrolyte addition. First and foremost, graphite is de-lithiated, whereas the highly lithiated silicon phases are still detectable after electrolyte addition. The ^7Li NMR measurements showed the presence of Li metal for all pre-lithiated electrodes, even after electrolyte contact. Therefore, Li metal seems to be passivated, leading to a slower/hindered lithiation of the active materials.

Finally, the lateral and in-depth lithium distribution of the Si/Gr electrode was examined by Raman spectroscopy and LA-ICP-OES measurements. An obvious disadvantage of pre-lithiation by PLMP is the inhomogeneous distribution of Li metal at the surface. The presence of lithium beneath PLMP particles was shown in-depth of the electrode via LA-ICP-OES analyses. After electrolyte addition, lithium showed a more uniform distribution within the electrode. The lateral lithiation was further investigated via Raman spectroscopy, which showed the lithiation of silicon lateral from the PLMP particle. While silicon particles are mostly lithiated close to a PLMP particle in the dry state, the lithiation continues more peripheral from the PLMP particle after electrolyte contact.

Overall, this work points out the challenges for pre-lithiation of Si/Gr electrodes by Li metal powder in terms of homogeneity, especially in terms of homogeneous SEI formation. This study may pave the way for further tailoring and optimization of the pre-lithiation process. Various strategies to further improve the homogeneity of the pre-lithiation can be followed in future studies, such as improved application techniques of PLMP including electrode “slurry”-based techniques and surface application techniques, for example, (thermal) spraying, coating, and compaction or dry sieving techniques. In addition, the reduction of the PLMP particle size in combination with a more homogeneous surface distribution could increase the overall homogeneity of pre-lithiation. Nevertheless, it must be kept in mind that each approach offers certain advantages (e.g., improved homogeneity) and drawbacks (e.g., challenges in terms of safety).

4. Experimental Section

Silicon/Graphite Electrode Preparation: Silicon/graphite (Si/Gr) composite electrodes were prepared by mixing 90 wt% active material and 10 wt% PAA (Sigma Aldrich; average Mw 450,000) binder, which was lithiated through LiOH (Sigma Aldrich, purity: 99.5%). The Si/Gr active material consisted of a physical mixture of 40 wt% Si particles ($D_{\text{mean}} = 0.76 \mu\text{m}$, $D_{90} = 1.33 \mu\text{m}$, see also^[14a]; Wacker Chemie AG) and 60 wt% synthetic graphite (KS4, $D_{90} = 4.9 \mu\text{m}$, Imerys Graphite & Carbon). As this study specifically focuses on the pre-lithiation mechanism of silicon and graphite, no additional conductive carbon was used for the composite electrode. The electrode paste was homogenized using a high-energy dispersion step, conducted at a speed of 11000 rpm (Ultra-Turrax T-25; IKA) for 60 min. Afterward, the paste was coated onto copper foil (Carl Schlenk AG; thickness: 15 μm ; purity: >99.9%) using a doctor blade technique. A blade gap of 120 μm was chosen so that the electrodes exhibited an active mass loading of $\approx 2.3\text{--}2.5 \text{ mg cm}^{-2}$ ($3.8\text{--}4.1 \text{ mAh cm}^{-2}$). The electrode sheets were dried in a vacuum oven

at 80 °C in ambient air for 24 h, and circular electrodes ($\varnothing 15 \text{ mm}$) were punched out. Further, these electrodes were dried at 80 °C under reduced pressure (at least $\leq 0.05 \text{ mbar}$) for another 24 h.

Pre-Lithiation of Si/Gr Negative Electrodes: For pre-lithiation, the Si/Gr electrodes were precisely weighed before PLMP (China Energy Lithium Co., Ltd.) was homogeneously distributed with a spatula at the electrode surface. The amount of PLMP was calculated based on the theoretical capacity of 1655 mAh g^{-1} for the Si/Gr electrode, based on the theoretical capacities of Si (3579 mAh g^{-1}) and graphite (372 mAh g^{-1}). Different degrees of pre-lithiation were targeted, namely 25% (“PreLi25”), 50% (“PreLi50”) and 75% (“PreLi75”) of the Si/Gr electrode's theoretical capacity. First, the PLMP was pressure-activated by a pressing tool ($\approx 280 \text{ kg cm}^{-2}$) for 30 s. This process was performed under a dry air atmosphere (dew point at least $-60 \text{ }^{\circ}\text{C}$). After pressing, the time was recorded and the Si/Gr electrode was either directly analyzed in dry state or transferred to an argon-filled glove box (H_2O : $<0.1 \text{ ppm}$; O_2 : $<0.1 \text{ ppm}$). After a rest period of 24 h in dry state, some of the Si/Gr electrodes were placed into a $10 \times 5 \text{ cm}^2$ pouch bag and 200 μL of electrolyte were added for further pre-lithiation. The pouch bag was sealed under reduced pressure (10^{-1} mbar) to ensure a homogeneous electrolyte distribution. LP57 (BASF SE; purity: battery grade; 11.7 ppm H_2O determined by Karl-Fischer titration), which contains 1 M lithium hexafluorophosphate (LiPF_6) dissolved in ethylene carbonate and ethyl methyl carbonate in a ratio of 3:7 by weight, was used as electrolyte. The pre-lithiation procedure with electrolyte continued for another 48 h. For post-mortem analysis, the Si/Gr electrodes were washed with 400 μL of dimethyl carbonate (purity: battery grade) to remove all residues of the conducting salt, and dried in the vacuum chamber of the glove box.

Electrochemical Investigation of Pre-Lithiated Si/Gr Electrodes: All electrochemical investigations were carried out in a half-cell setup (three-electrode configuration; control of working electrode (WE) potential via reference electrode (RE)) in Swagelok-type T-cells using Li metal foil (Albemarle; purity: battery grade) as counter electrode (CE) and RE. A three-layered $\varnothing 13 \text{ mm}$ separator (FS 2190, Freudenberg Performance Materials) was placed between WE and CE and a three-layered $\varnothing 8 \text{ mm}$ separator (FS 2190) was used for the RE. All cells were filled with 120 and 80 μL of electrolyte (LP57) for the WE/CE and RE separators, respectively. All electrodes had a rest period of 24 h after pressure-induced activation (in dry state) before being assembled into Swagelok the cell and having contact with electrolyte.

In a first electrochemical investigation, the open circuit potentials (E_{OCP}) versus $\text{Li}|\text{Li}^+$ of the pre-lithiated Si/Gr electrodes were measured for 200 h (Figure 2a). For galvanostatic experiments, the three-electrode cells were cycled in a WE potential range of 0.05 to 1.2 V versus $\text{Li}|\text{Li}^+$ after a rest period of 48 h of the three-electrode cell (Figure S2, Supporting Information). The pristine and pre-lithiated Si/Gr electrodes were cycled for 10 cycles with a charge/discharge rate of 0.1 C ($\approx 0.4 \text{ mA cm}^{-2}$; 1C corresponds to 1655 mA g^{-1}), starting with the lithiation to a potential of 0.05 V versus $\text{Li}|\text{Li}^+$. After the WE potential was reached, the WE potential was kept constant until a current of $\leq 0.05 \text{ C}$ ($\approx 81 \text{ mA g}^{-1}$) was reached. The C-rate and specific current for the Si/Gr electrodes was calculated based on the theoretical capacity of 1655 mAh g^{-1} . All electrochemical measurements were carried out on a Maccor series 4000 battery tester at room temperature. For cyclic voltammetry measurements (Figure 2b), the Si/Gr || Li metal cells were also operated in a WE potential range of 0.05 and 1.2 V versus $\text{Li}|\text{Li}^+$ (scan rate: 0.1 mV s^{-1}), after a resting period of 48 h.

Characterization Methods: To investigate the Si/Gr electrode morphology after pre-lithiation, a SEM (Carl Zeiss AURIGA; Carl Zeiss Microscopy GmbH) equipped with a field emission gun was used. The SEM images were taken using a working distance between 3.5 to 4 mm and an accelerating voltage of 3 kV. Energy dispersive X-ray spectroscopy was measured with a X-MAX 80 mm^2 detector to evaluate the elemental composition of the samples. The spectra were evaluated with the INCA software (Oxford Instruments). For the cross-section investigations, the pre-lithiated Si/Gr electrodes were sliced using a razor blade.

The bulk structure of the pre-lithiated Si/Gr electrodes was analyzed by ex situ Raman spectroscopy, in situ XRD and ex situ solid-state ^7Li

NMR spectroscopy. To record XRD patterns and to determine the lithiated graphite and silicon phases and lattice parameters, a Bruker D8 Advance X-ray diffractometer (Bruker AXS GmbH) with a Cu-K α wavelength of 0.154 nm and with a divergence slit of 0.5° was used. XRD analyses of the Si/Gr electrodes were carried out using an in situ cell with a 10 mm inspection area (ECC Opto Std; EL-Cell). The electrodes were prepared as described above, while the Si/Gr composite material faced a beryllium (Be) disk (thickness: 250 μ m; Brush Wellmann GmbH). The XRD measurements were conducted in the range from 10° to 40° with a step size of 0.04° and a dwell time of 1.8 s. The individual XRD measurements started each 25 min for 24 h in the dry state. Afterward, the electrolyte was filled into the cells and the measurements were resumed for another 48 h with the same Si/Gr electrode. After conducting the experiment, a full XRD pattern was recorded from 10° to 70° with a step size of 0.03° and a dwell time of 1.5 s, from which the copper (110) reflex was used for referencing the patterns.

Raman spectra of pre-lithiated Si/Gr electrodes were recorded with a Raman microscope (Bruker SENTERRA) equipped with a 532 nm laser and using 0.2 mW of excitation power. An objective with a 50 \times magnification and a grating of 400 grooves mm⁻¹ was chosen for the measurements. Five integrations with an integration time of 30 s were used to collect the spectra. A mapping close to a Li metal particle (PLMP) was produced by a rectangle of 60 μ m in length and 28 μ m in width, with a total measurement of 96 spectra (see Figure 7). These spectra were split up in 12 measurements, 5 μ m apart in line of longitude and eight measurements in line of latitude with a distance of 3.5 μ m in between. The measurements were averaged parallel to latitude to eliminate fluctuations and to ensure reproducibility. The same cell setup as for the XRD studies (ECC Opto Std; EL-Cell) was used as a sample holder with a glass observation window to avoid any contamination. The first mapping was recorded directly after pressure-induced activation, the second mapping after 24 h in dry-state and the final one after 48 h electrolyte contact.

The sample preparation for the solid-state ⁷Li NMR measurements, including grinding, diluting, and packing the samples into zirconium dioxide (ZrO₂) rotors, was performed in an argon-filled glove box. The pre-lithiated Si/Gr electrodes were scratched from the Cu current collector using a ceramic scalpel, grinded, and diluted 1:4 by weight with MgO to prevent Eddy currents and, thereby additional heating of the sample during the NMR measurement. All static ⁷Li NMR spectra were recorded on a 500 MHz Bruker DSX spectrometer equipped with a 11.75 T ($\nu_L(^7\text{Li}) = 194.94$ MHz) wide bore magnet using a 2.5 mm Bruker MAS probe (VTN design). The ⁷Li chemical shifts were referenced to a 1 M LiCl solution and its isotropic chemical shift is set $\delta_{\text{iso}} = 0$ ppm. For the investigation of the lithiated graphite and silicon species, one-pulse ⁷Li NMR experiments were performed using a radio-frequency field strength (ν_{RF}) of 100 kHz. The recycle delay was set to 120 s to ensure full T₁ relaxation after each recorded transient. A total number 160 transients was used for each ⁷Li NMR spectrum. Data processing was performed using the TopSpin and DmFit software packages.^[31]

LA-ICP-OES measurements were performed using the LSX-213 laser ablation system (Teledyne CETAC) coupled to an ARCOS (Spectro Analytical Instruments GmbH) ICP-OES system with a radial positioned plasma torch. The LA system was controlled by the software DigiLaz III (version 3.2.3, Teledyne CETAC). The software Smart Analyzer Vision (version 5.01.0927, Spectro Analytical Instruments) controlled the ICP-OES system.^[32] The scans were performed using a circular ablation spot (100 μ m diameter), a scanning speed of 200 μ m s⁻¹, a laser frequency of 10 Hz and a laser energy of ≈ 1 mJ. Helium (99.9999%, Westfalen AG) was used as the laser ablation carrier gas, with a gas flow of 900 mL min⁻¹. The laser ablation carrier gas was mixed with a wet nebulizer aerosol before entering the plasma torch. The ICP-OES measurements were carried out using an RF power of 1500 W, a total argon flow of 13.8 L min⁻¹ (nebulizer gas flow: 0.6 L min⁻¹, auxiliary gas flow: 1.2 L min⁻¹, cooling gas flow: 12 L min⁻¹) and a torch with an inner diameter of 1.8 mm. Following emission lines were recorded: Li (670.237 nm), Cu (324.754 nm), and C (193.091 nm) as an internal standard.

Supporting Information

Supporting Information is available from the Wiley Online Library or from the author.

Acknowledgements

P.B. and M.M. contributed equally to this work. The authors thank the European Union for funding this work in the project “SeNSE”: This project has received funding from the European Union’s Horizon 2020 research and innovation program under grant agreement No 875548. The authors also thank the Federal Ministry of Education and Research (BMBF) for funding this work in the project “PräLi” (03XP0238C) within the ProZell competence cluster. Further, the authors thank the Wacker Chemie AG for Si material supply. Andre Bar is acknowledged for his graphical support.

Open access funding enabled and organized by Projekt DEAL.

Conflict of Interest

The authors declare no conflict of interest.

Data Availability Statement

Data available on request from the authors.

Keywords

active lithium loss, lithium ion batteries, passivated lithium metal powder, pre-lithiation, silicon/graphite anodes

Received: March 20, 2021

Revised: May 3, 2021

Published online: May 13, 2021

- [1] a) P. Meister, H. Jia, J. Li, R. Kloepsch, M. Winter, T. Placke, *Chem. Mater.* **2016**, *28*, 7203; b) R. Schmich, R. Wagner, G. Hörpel, T. Placke, M. Winter, *Nat. Energy* **2018**, *3*, 267.
- [2] a) J. Graetz, C. C. Ahn, R. Yazami, B. Fultz, *Electrochem. Solid-State Lett.* **2003**, *6*, A194; b) M. N. Obrovac, V. L. Chevrier, *Chem. Rev.* **2014**, *114*, 11444; c) X. Zuo, J. Zhu, P. Müller-Buschbaum, Y.-J. Cheng, *Nano Energy* **2017**, *31*, 113; d) F. Holtstiege, A. Wilken, M. Winter, T. Placke, *Phys. Chem. Chem. Phys.* **2017**, *19*, 25905.
- [3] a) M. Ashuri, Q. He, L. L. Shaw, *Nanoscale* **2016**, *8*, 74; b) X. H. Liu, L. Zhong, S. Huang, S. X. Mao, T. Zhu, J. Y. Huang, *ACS Nano* **2012**, *6*, 1522.
- [4] F. Holtstiege, P. Bärmann, R. Nölle, M. Winter, T. Placke, *Batteries* **2018**, *4*, 4.
- [5] a) Y. Li, B. Fitch, *Electrochem. Commun.* **2011**, *13*, 664; b) N. Liu, L. Hu, M. T. McDowell, A. Jackson, Y. Cui, *ACS Nano* **2011**, *5*, 6487; c) K. H. Kim, J. Shon, H. Jeong, H. Park, S. J. Lim, J. S. Heo, *J. Power Sources* **2020**, *459*, 228066.
- [6] A. Shellikeri, V. G. Watson, D. L. Adams, E. E. Kalu, J. A. Read, T. R. Jow, J. P. Zheng, *ECS Trans.* **2017**, *77*, 293.
- [7] C. R. Jarvis, M. J. Lain, M. V. Yakovleva, Y. Gao, *J. Power Sources* **2006**, *162*, 800.
- [8] B. Xiang, L. Wang, G. Liu, A. M. Minor, *J. Electrochem. Soc.* **2013**, *160*, A415.
- [9] a) J. Heine, S. Krüger, C. Hartnig, U. Wietelmann, M. Winter, P. Bieker, *Adv. Energy Mater.* **2014**, *4*, 1300815; b) Q. Pan, P. Zuo, T. Mu, C. Du, X. Cheng, Y. Ma, Y. Gao, G. Yin, *J. Power Sources* **2017**, *347*, 170.

- [10] a) J. Heine, U. Rodehorst, X. Qi, J. P. Badillo, C. Hartnig, U. Wietelmann, M. Winter, P. Bieker, *Electrochim. Acta* **2014**, *138*, 288; b) M. Marinaro, M. Weinberger, M. Wohlfahrt-Mehrens, *Electrochim. Acta* **2016**, *206*, 99; c) G. Ai, Z. Wang, H. Zhao, W. Mao, Y. Fu, R. Yi, Y. Gao, V. Battaglia, D. Wang, S. Lopatin, G. Liu, *J. Power Sources* **2016**, *309*, 33.
- [11] F. Holtstiege, R. Schmuck, M. Winter, G. Brunklaus, T. Placke, *J. Power Sources* **2018**, *378*, 522.
- [12] H. Xu, S. Li, C. Zhang, X. Chen, W. Liu, Y. Zheng, Y. Xie, Y. Huang, J. Li, *Energy Environ. Sci.* **2019**, *12*, 2991.
- [13] M. W. Forney, M. J. Ganter, J. W. Staub, R. D. Ridgley, B. J. Landi, *Nano Lett.* **2013**, *13*, 4158.
- [14] a) P. Bärnmann, M. Diehl, L. Göbel, M. Ruttert, S. Nowak, M. Winter, T. Placke, *J. Power Sources* **2020**, *464*, 228224; b) J. Zhang, Z. Shi, C. Wang, *Electrochim. Acta* **2014**, *125*, 22.
- [15] P. Bärnmann, B. Krueger, S. Casino, M. Winter, T. Placke, G. Wittstock, *ACS Appl. Mater. Interfaces* **2020**, *12*, 55903.
- [16] a) D. S. M. Iaboni, M. N. Obrovac, *J. Electrochem. Soc.* **2015**, *163*, A255; b) P. Novák, D. Goers, M. E. Spahr, in *Carbons for electrochemical Energy Storage and Conversion Systems* (Eds: F. Beguin, E. Frackowiak), CRC Press, Boca Raton, FL **2010**, p. 263.
- [17] a) J. R. Dahn, R. Fong, M. J. Spoon, *Phys. Rev. B* **1990**, *42*, 6424; b) B. Key, R. Bhattacharyya, M. Morcrette, V. Seznéc, J.-M. Tarascon, C. P. Grey, *J. Am. Chem. Soc.* **2009**, *131*, 9239.
- [18] Y. Kubota, M. C. S. Escañó, H. Nakanishi, H. Kasai, *J. Appl. Phys.* **2007**, *102*, 053704.
- [19] a) H. Gao, L. Xiao, I. Plümel, G.-L. Xu, Y. Ren, X. Zuo, Y. Liu, C. Schulz, H. Wiggers, K. Amine, Z. Chen, *Nano Lett.* **2017**, *17*, 1512; b) S. Tardif, E. Pavlenko, L. Quazuguel, M. Boniface, M. Maréchal, J.-S. Micha, L. Gonon, V. Mareau, G. Gebel, P. Bayle-Guillevaud, F. Rieutord, S. Lyonard, *ACS Nano* **2017**, *11*, 11306.
- [20] a) M. Letellier, F. Chevallier, F. Béguin, *J. Phys. Chem. Solids* **2006**, *67*, 1228; b) M. Letellier, F. Chevallier, M. Morcrette, *Carbon* **2007**, *45*, 1025; c) N. M. Trease, T. K. J. Koester, C. P. Grey, *Interface Mag.* **2011**, *20*, 69.
- [21] J. L. Lorie Lopez, P. J. Grandinetti, A. C. Co, *J. Mater. Chem. A* **2019**, *7*, 10781.
- [22] a) L. A. Huff, H. Tavassol, J. L. Esbenshade, W. Xing, Y.-M. Chiang, A. A. Gewirth, *ACS Appl. Mater. Interfaces* **2016**, *8*, 371; b) J.-H. Trill, C. Tao, M. Winter, S. Passerini, H. Eckert, *J. Solid State Electrochem.* **2010**, *15*, 349.
- [23] B. Key, M. Morcrette, J.-M. Tarascon, C. P. Grey, *J. Am. Chem. Soc.* **2011**, *133*, 503.
- [24] R. Bhattacharyya, B. Key, H. Chen, A. S. Best, A. F. Hollenkamp, C. P. Grey, *Nat. Mater.* **2010**, *9*, 504.
- [25] N. M. Trease, L. Zhou, H. J. Chang, B. Y. Zhu, C. P. Grey, *Solid State Nucl. Magn. Reson.* **2012**, *42*, 62.
- [26] a) M. Holzapfel, H. Buqa, L. J. Hardwick, M. Hahn, A. Würsig, W. Scheifele, P. Novák, R. Kötz, C. Veit, F.-M. Petrat, *Electrochim. Acta* **2006**, *52*, 973; b) R.-p. Wang, G.-w. Zhou, Y.-l. Liu, S.-h. Pan, H.-z. Zhang, D.-p. Yu, Z. Zhang, *Phys. Rev. B* **2000**, *61*, 16827.
- [27] a) L. Hardwick, H. Buqa, P. Novak, *Solid State Ionics* **2006**, *177*, 2801; b) A. Sadezky, H. Muckenhuber, H. Grothe, R. Niessner, U. Pöschl, *Carbon* **2005**, *43*, 1731.
- [28] H. Li, X. Huang, L. Chen, G. Zhou, Z. Zhang, D. Yu, Y. Jun Mo, N. Pei, *Solid State Ionics* **2000**, *135*, 181.
- [29] A. Krause, O. Tkacheva, A. Omar, U. Langklotz, L. Giebeler, S. Dörfler, F. Fauth, T. Mikolajick, W. M. Weber, *J. Electrochem. Soc.* **2019**, *166*, A5378.
- [30] T. Schwieters, M. Evertz, M. Mense, M. Winter, S. Nowak, *J. Power Sources* **2017**, *356*, 47.
- [31] D. Massiot, F. Fayon, M. Capron, I. King, S. L.e Calvé, B. Alonso, J.-O. Durand, B. Bujoli, Z. Gan, G. Hoatson, *Magn. Reson. Chem.* **2002**, *40*, 70.
- [32] C. Lürenbaum, B. Vortmann-Westhoven, M. Evertz, M. Winter, S. Nowak, *RSC Adv.* **2020**, *10*, 7083.